PERGAMON

Journal of Structural Geology 24 (2002) 963–977

JOURNAL OF STRUCTURAL GEOLOGY

www.elsevier.nl/locate/jstrugeo

Deformation in Neogene sediments of the Sorbas and Vera Basins (SE Spain): constraints on simple-shear deformation and rigid body rotation along major strike-slip faults

R. Jonk*, C. Biermann

Department of Earth-Sciences, Vrije Universiteit Amsterdam, De Boelelaan 1085, 1081 HV Amsterdam, The Netherlands

Received 28 July 2000; revised 17 August 2001; accepted 30 August 2001

Abstract

Detailed structural analyses are presented of the Neogene Sorbas Basin adjacent to the E–W striking Gafarillos fault zone and the Vera Basin adjacent to the 020° striking Palomares fault zone in southeastern Spain. A stress regime with an E–W oriented subhorizontal maximum principal stress (σ_1) existed in pre-Tortonian (>11.3 Ma) time. A strike-slip regime with NW–SE oriented compression during Tortonian and earliest Messinian time caused dextral displacement along the E–W trending Gafarillos fault of approximately 10 km. Structural analysis indicates that most displacement took place in the Early Tortonian. Deformational patterns within the adjacent pull-apart basin reflect a dextral simple shear-zone of at least 500 m width. Kinematical analysis of folds in the Sorbas Basin suggests, however, that rotational effects are largely caused by rigid-body rotation without much internal deformation. Sinistral strike-slip displacements occurred along the Palomares fault zone under the influence of the same stress-regime.

An abrupt change in the orientation of the stress field to N–S directed compression in earliest Messinian time (6.5 Ma) caused the termination of displacements along the Gafarillos fault zone, whereas the 020° trending Palomares fault zone continued to accumulate sinistral strike-slip displacements of about 25 km. Volcanism occurred along splays of the fault zone. A wider shear-zone of a few kilometers width evolved, in which considerable anti-clockwise rotation of folds occurred. Kinematic analysis of these folds shows that these rotational effects are again dominantly rigid-body rotations. Assuming rotations are merely caused by simple-shear deformation overestimates the amounts of strain. A better way to deal with simple-shear deformation is to compare observed shortening caused by folding with the magnitude of rotation of fold-hinges.

Keywords: Paleostress analysis; Neogene pull-apart basins; Strike-slip faults; Simple shear deformation; Betic Cordilleras

1. Introduction

Finite strain within shear-zones may be a combination of simple shear deformation, pure shear deformation, and volume change. Many previous authors have elaborated on this (e.g. Ramsay, 1980; Sanderson and Marchini, 1984; Fossen and Tikoff, 1993) and focused on factorization into simple shear and pure shear components (Sanderson and Marchini, 1984; Fossen and Tikoff, 1993). Factorization into simple and pure shear components of strain will allow the distinction between transpressional and transtensional tectonics (Fossen and Tikoff, 1993). However, to complicate matters, rigid body rotations without internal deformation may occur within shear-zones (Ramsay and Huber, 1987). Rigid body rotations have not been incorporated in the factorization of different components of strain and rotation within shear-zones. If, however, rotations of markers (such as fold-hinge lines or foliations) are used to deduce amounts of shear strain, they will be overestimated when rigid body rotations are present.

In this paper, we analyze the orientations of fold hinge lines and the amounts of shortening accommodated by folds within strike-slip shear-zones in the Betic Cordilleras in SE Spain. Several differently oriented brittle-ductile strike-slip shear-zones (Ramsay, 1980) occur in the area. Huibregtse et al. (1998) previously recognized folds along some of the strike-slip faults as being related to simple shear deformation and Weijermars (1987) used deflections of fold-hinge-lines near major strike-slip faults to deduce amounts of shear strain. By comparing rotations of fold-hinge lines near strike-slip faults with the shortening accommodated by folds, we can separate simple shear deformation and rigid

* Corresponding author. Present address: Injected Sands Group, Department of Geology and Petroleum Geology, University of Aberdeen, Aberdeen AB24 3UE, UK. Tel.: +44-(0)1224-273-435; fax: +44-(0)1224-278585.

E-mail address: r.jonk@abdn.ac.uk (R. Jonk).

0191-8141/02/$ - see front matter
PII: S0191-8141(01)00107-9

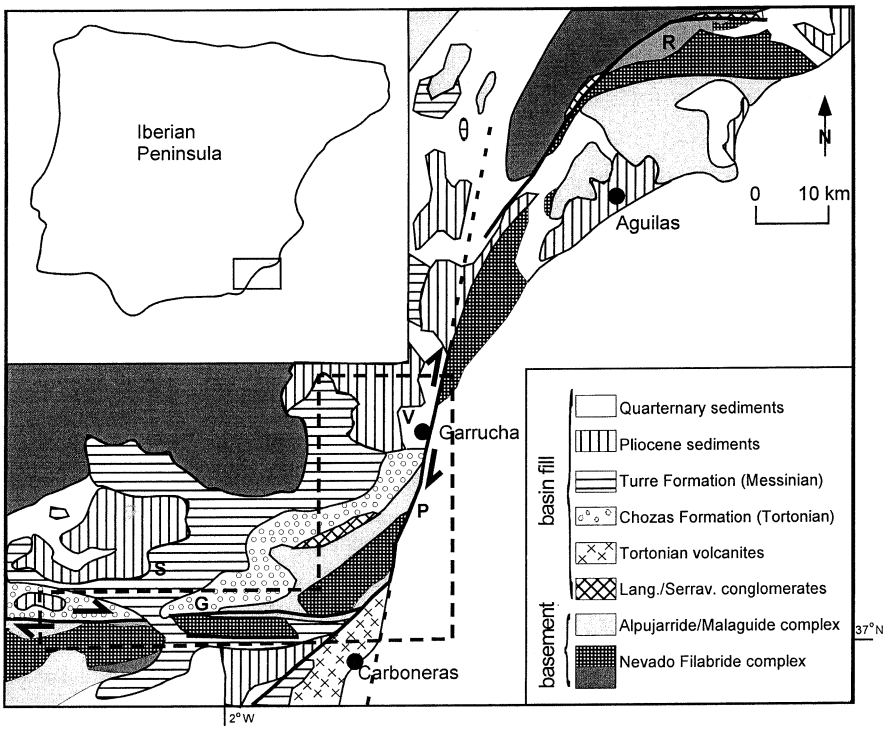

Fig. 1. Outline of the main stratigraphic and structural patterns in the southeastern Internal Betic Cordilleras; G = Gafarillos fault, P = Palomares fault, R = Ramonete fault, S = Sorbas Basin, V = Vera Basin. The dashed box indicates the location of Fig. 4.

body rotation. The possibility of a component of pure shear deformation will be evaluated as well.

2. Regional geological setting

2.1. Geological evolution of the Betic Cordilleras

The Betic Cordilleras in southeastern Spain are made up of a northern External Zone and a southern Internal Zone. The External Zone represents the passive continental margin of Iberia (Garcia-Hernandez et al., 1980) and comprises sediments of Late Jurassic to Paleogene age. The Internal Zone consists of a stack of metamorphic nappes (Egeler and Simon, 1969) of Paleozoic to Triassic age and Neogene sedimentary basins (Fig. 1). The nappes represent the deep structure of a Late Cretaceous subduction complex (Bakker et al., 1989). This subduction complex, originally located several hundreds of kilometers to the east, became dispersed during Late Oligocene to earliest Miocene extension in the western Mediterranean and the associated opening of the Provencal Basin (Sanz de Galdeano and Vera, 1992; Geel, 1995). Neogene convergence in southeastern Spain is associated with basin formation and basement uplift under the influence of major strike-slip deformation (Biermann, 1995). This last major tectonic phase resulted in a mountain belt that presently forms a discontinuous mountain-chain, separated by basins of Miocene to Quaternary age. These basins are commonly bounded by large strike-slip fault zones, adjacent to which sediments are strongly deformed. The pull-apart origin of these basins is clearly demonstrated by the character of the basin fill. Proximal provenance of high-energy mass-flow deposits indicate areas of local basement uplift and erosion adjacent to areas with rapid subsidence and deposition features characteristic of a pull-apart origin (Sylvester, 1988). The Neogene evolution of southeastern Spain shows a complicated interaction of activity and inactivity of the major strike-slip fault zones. This tectonic evolution has been documented in the sediments within the Neogene basins.

2.2. Geological setting of the basin areas

The sedimentary sequences indicate that the basins were discrete depocentres at least from the Tortonian onward (Weijermars et al., 1985). Older Langhian–Serravallian (>11.3 Ma) deposits cannot be interpreted unambiguously. Continental conglomerates of this age clearly show local source-areas, while yellow marls may have been deposited in a larger regional basin. Onset of strike-slip deformation at the beginning of the Tortonian (11.3 Ma) caused the different basins to become isolated. Detailed descriptions of the stratigraphy of the Vera and Sorbas Basins have been presented by Völk and Rondeel (1964), Völk (1967), Weijermars et al. (1985) and Mather and Harvey (1995). The Sorbas Basin is bounded to the south by the Gafarillos fault zone and separates metamorphic basement of the

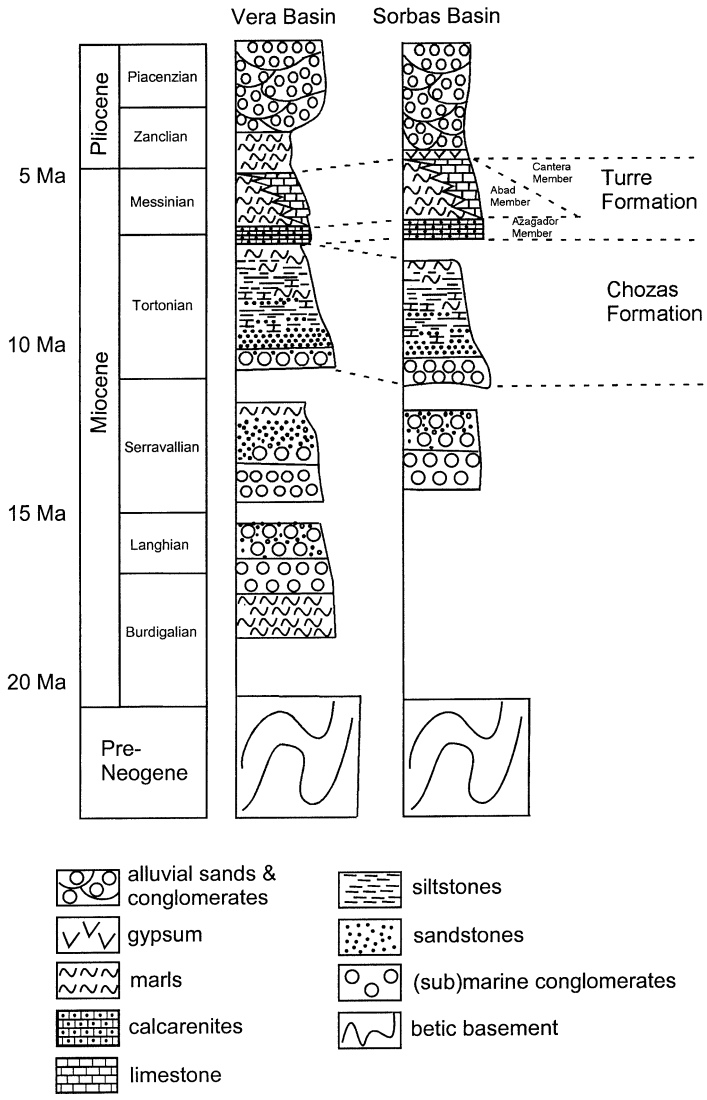

Fig. 2. General stratigraphic overview of the Vera and Sorbas Basins. Only formations and members mentioned in the text have been indicated. Note that time-spans of deposition are indicated and not stratigraphic thicknesses (modified after Huibregtse et al., 1998).

Sierra de Alhamilla from Tortonian and younger sediments. The Sierra de Alhamilla forms an east–west anticlinorium plunging to both sides. The Sierra consists of three major tectonic nappes. The core of the metamorphic basement comprises a series of micaschist and quartzites, representing the Nevado–Filabride complex (Egeler and Simon, 1969) and is overlain by Triassic low-greenschist facies quartzites and carbonates of the Alpujarride complex. Small occurrences of the Malaguide complex, containing non-metamorphic Paleozoic and Triassic clastics, are present on top of the Alpujarride rocks.

The Neogene stratigraphy of the Sorbas Basin is summarized in Fig. 2. The oldest sediments are Serravallian (11.3–15 Ma) continental conglomerates with dominantly Alpujarride and Malaguide detritus. These conglomerates are unconformably overlain by Tortonian (11.3–6.3 Ma) turbidites of a south-directed submarine fan system derived from the Sierra de los Filabres (Kleverlaan, 1989; Haughton, 1994). The total sequence represents a transition from coastal to deeper waters. The presence of synsedimentary slumps and turbidites indicates major tectonic activity during the Early Tortonian. A second transgressive cycle started in the Messinian (<6.3 Ma) with a sequence of onlapping shallow marine conglomerates, which upward and basinward grade into marine marls. Large barrier reefs mark the margins of the Messinian seas (Weijermars et al., 1985) and are the oldest rocks unaffected by the Gafarillos fault zone. Younger sediments, including large gypsum deposits of the Messinian Salinity Crisis, were not investigated near the fault-contact.

The Palomares fault zone runs along the eastern boundary of the Vera Basin. The Neogene stratigraphy of the basin is summarized in Fig. 2. The oldest sediments are open marine Late Burdigalian (16–19.2 Ma) marls and thin interbedded limestones and marls (Alamo series; Völk and Rondeel, 1964). Deposition of these open marine sediments over

large areas pre-date differentiation of the Betic depositional area.

Strike-slip controlled basin subsidence and basement uplift started during the Mid Miocene. The late Burdigalian marls are unconformably overlain by Middle Miocene marine conglomerates and sandstones. The conglomerates are dominated by detritus from the local basement complexes indicating uplift and erosion of the nearby Sierras. The top of the Middle Miocene series is characterized by deep marine yellow marls of Serravallian (11.3–15 Ma) age. These marls are unconformably overlain by Tortonian mass flows, well-bedded turbidites and deep marine marls of the Chozas Formation (Völk and Rondeel, 1964). They contain detritus of the deeper-seated Nevado–Filabride nappes in the Sierra de los Filabres. This presents evidence for uplift and erosion that cuts deeply into the basement nappes (Kleverlaan, 1989). Early Messinian sedimentation in the Vera Basin starts with a transgressive sequence of on-lapping coastal marine calcarenites that unconformably overly Tortonian turbidites. As in the Sorbas Basin, these calcarenites grade upward and basinward into marine pelagic marls. The basin margins are bounded by barrier reef deposits. In the center of the Vera Basin, turbidites occur in the top of these pelagic marls. The Messinian strata are unconformably overlain by Pliocene marls and overlying fan delta and gravel beach deposits of the Cuevas Formation (Völk, 1967; Postma and Roep, 1985; Fortuin et al., 1995).

2.3. Location of the study areas

The two strike-slip faults selected for detailed structural analysis are (Fig. 1):

1. The E–W striking dextral Gafarillos fault zone, separating the Sierra Alhamilla and the Sierra Cabrera by approximately 10 km. The displacement history of this fault zone is recorded in the Sorbas Basin, on the northern side of this fault zone.
2. The 020° trending Palomares fault zone that offsets the basement structure of the Sierra Cabrera and Sierra Almagrera in a total sinistral displacement of approximately 25 km (Völk, 1967).

The displacement history of this fault zone is recorded in the Neogene sediments of the Vera Basin, situated at the western side of this fault zone.

3. Paleostress analysis

3.1. Methodology

The investigated areas are characterized by numerous differently oriented striated faults, which makes them well suited for paleostress analysis. Stress analysis is based on the assumption that both direction and sense of movement on a fault plane are completely determined by the state of stress (Bott, 1959). Slip on a fault plane takes place in the direction of the resolved shear stress vector on that plane, as determined from the mean stress deviator. In paleostress analysis, the inverse problem is solved. When orientations and senses of movement on sufficient fault planes with different orientations are known, it is possible to compute the reduced stress tensor, expressed in the orientations of the principal axes of stress ($\sigma_1 > \sigma_2 > \sigma_3$) and by the relative magnitudes of the principal stress axes, expressed in the stress ratio R, defined as:

$$R = (\sigma_2 - \sigma_3)/(\sigma_1 - \sigma_3) \quad (1)$$

Magnitudes of principal stresses cannot be determined from fault-slip data alone. Information on the rheological properties of the investigated rocks as well as on lithostatic pressures during faulting are needed to determine absolute stress-magnitudes (Angelier, 1989). Tensors discussed in this paper are always reduced tensors. The quality of the fit of the theoretical tensor to the selected subset is expressed by the slip deviation α. This parameter represents the angle of deviation between the calculated shear stress vector and the observed striations of the fault. Striations that deviate more than 30° were in all cases rejected for the calculation of the stress tensor. The α-angle is the parameter optimized during the calculations. The relative quality of tensors is expressed in the Tensor Quality Rank (*TQR*), which is defined by Delvaux (1994) as:

$$TQR = (N(N/N_{\text{tot}}))/\alpha \quad (2)$$

with N_{tot} being the total number of measurements at one stress site and N the number of faults that fitted within the calculated regime. An arbitrary scale from A to C (Delvaux et al., 1997) has been coupled to this parameter in order to make the quality of different sites easily comparable. Tensors of high quality (A) correspond to a *TQR* larger than 1.5, quality B corresponds to a *TQR*between 0.5 and 1.5 and C to a *TQR* below 0.5. Tensors with *TQR* below 0.5 were considered unreliable and have not been incorporated in the regional synthesis. The paleostress method assumes: tectonic events are characterized by one regional homogeneous stress-regime; broken rock-bodies are thought to be composed of rigid parts, sliding along each other with a constant friction coefficient; during or after faulting, no rotations should have occurred. Despite these assumptions, previous paleostress analyses have given reliable and reproducible results (e.g. Stapel et al., 1996; Huibregtse et al., 1998).

3.2. Results

A total of 1360 measurements of striated fault planes from 46 sites along both strike-slip faults were collected in both pre-Neogene basement and in Neogene sediments of Serravallian to Pliocene age. All stress-sites are located outside the central fault zones in order to avoid effects of

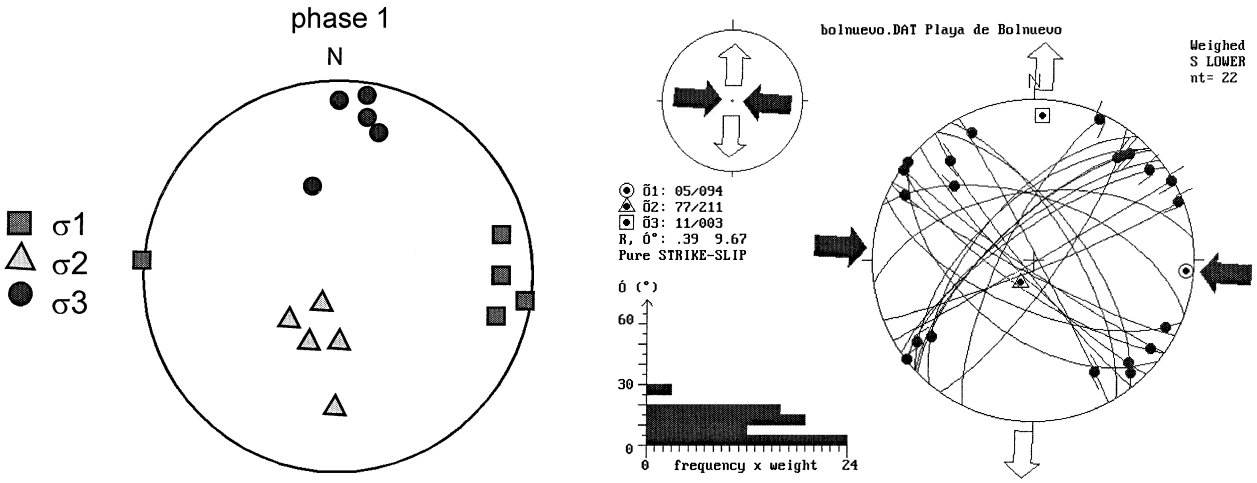

Fig. 3. Stress-tensors of phase 1 (left) with an example of a phase 1 stress tensor (right). Relative ages have been determined, so that phase 1 is the oldest and phase 4 is the youngest.

local stress perturbations within and near the fault zones. A stress-site consists of numerous (preferably more than 20) differently oriented fault planes within a radius of less than about 100 m. Both ridges and grooves and slickenfibers were used as fault-slip indicators. The best fit tensor (the one generating the highest *TQR*) for a data-set is then calculated. Stress-sites were measured in lithologies of varying ages, in order to discriminate between temporal and spatial variations in the stress field. The fault-slip data show a wide variety in orientation of both fault-planes and striae, although the majority of the measured fault-slip data are strike-slip faults.

3.2.1. Stress-tensors with an E–W trending σ_1 (phase 1 tensors)

Examples of stress tensors with a subhorizontal E–W trending σ_1 and a subhorizontal σ_3 were collected only in five sites (Fig. 3). Phase 1 tensors have only been detected in the northeastern parts of the investigated area, near the interaction of the Ramonete fault zone with the Palomares fault zone (Fig. 1). These tensors were only observed in Alpujarride and Nevado–Filabride basement and in Langhian to Serravalian conglomerates and are not present in Tortonian and younger sediments and thus clearly show that they represent a stress-regime that existed in pre-Tortonian time.

3.2.2. Stress-tensors with a NW–SE trending σ_1 (phase 2 tensors)

A total number of 16 tensors fit within a tectonic phase, dominated by a subhorizontal NW–SE trending maximum compressive principal axis of stress σ_1 and a subhorizontal NE–SW trending minimum principal axis of stress σ_3 (Table 1; Fig. 4a). These phase 2 tensors were, in most cases, detected in the Sorbas Basin, along the Gafarillos fault zone. Phase 2 tensors are present in pre-Neogene

Table 1
All tensors of phase 2. Symbols explained in text

Lithology	Structural location	N	N_{tot}	σ_1	σ_2	σ_3	α	TQR	Rank
Tort. marls	Gafarillos fault	12	23	151/23	258/33	033/50	6.15	1.02	B
Alp. basement	Gafarillos fault	16	27	332/02	078/84	242/05	5.74	1.49	B
Tort. turbidites	Gafarillos fault	11	27	321/30	053/05	150/60	8.74	0.52	B
Alp. basement	Gafarillos fault	13	24	317/50	208/13	110/30	8.45	0.86	B
Tort. turbidites	Gafarillos fault	12	18	305/23	140/67	037/05	3.56	1.71	A
Tort. turbidites	Gafarillos fault	12	15	123/14	359/67	217/19	7.32	1.31	B
Tort. turbidites	Gafarillos fault	42	50	144/13	033/60	240/30	9.68	3.54	A
Tort. turbidites	Gafarillos fault	23	32	119/02	211/61	028/28	8.56	1.51	A
Tort. turbidites	Gafarillos fault	19	27	301/30	165/60	045/18	10.3	1.30	B
Alp. basement	Gafarillos fault	11	20	312/26	164/59	045/20	10.7	0.53	B
Alp. basement	Gafarillos fault	12	21	315/16	061/58	210/23	7.04	0.76	B
Alp. basement	Unknown fault	29	62	115/25	334/62	213/15	9.52	1.45	B
Alp. basement	Palomares fault	29	50	149/28	286/59	048/20	9.73	1.75	A
Tort. turbidites	Palomares fault	17	25	331/12	080/78	240/08	9.45	1.56	A
Alp. basement	Palomares fault	11	30	298/09	137/80	029/03	7.34	0.55	B
Tort. turbidites	Gafarillos fault	14	18	287/14	026/30	178/58	10.2	1.07	B

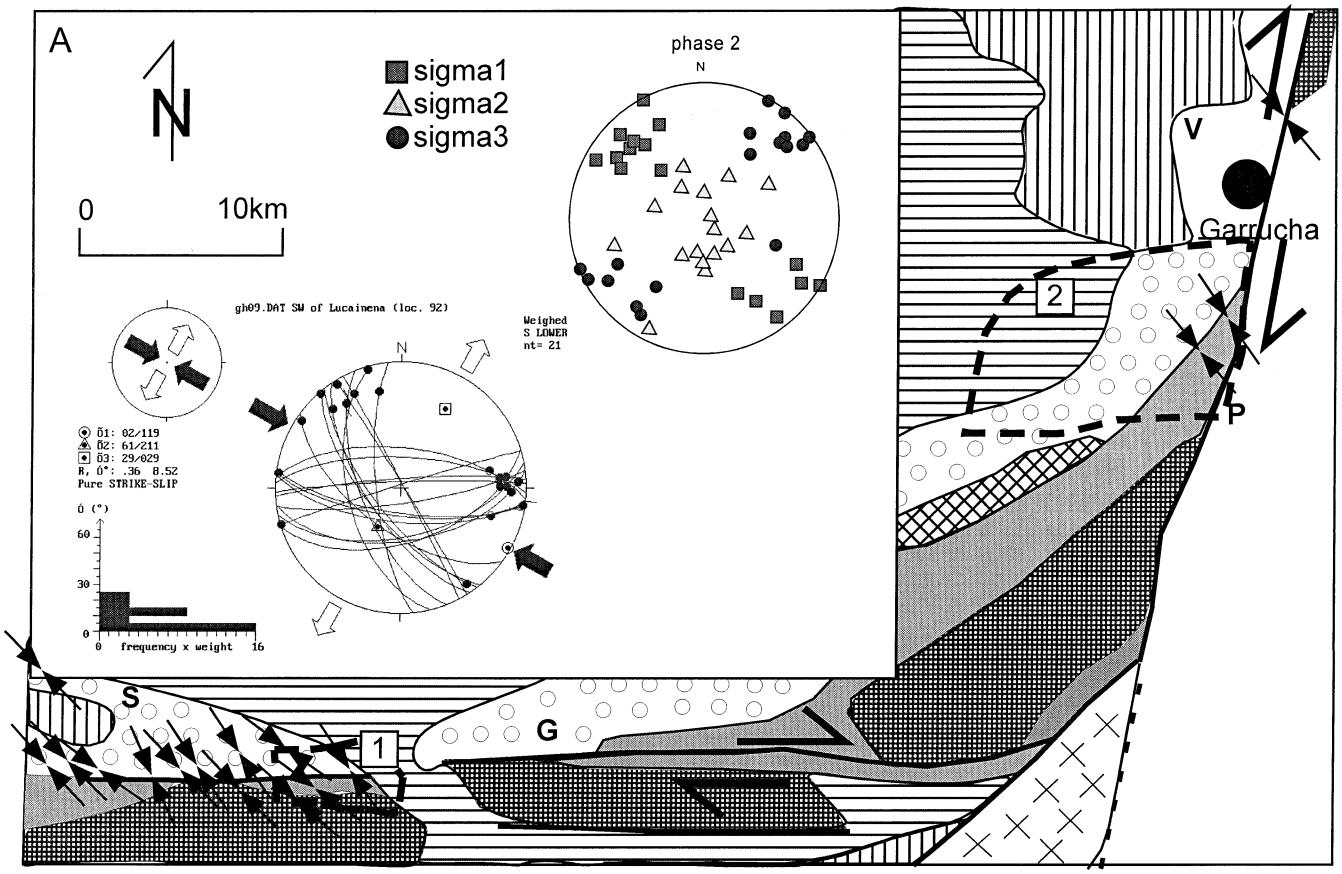
A
sigma1
sigma2
sigma3
0
10km
phase 2
N
gh09.DAT SW of Lucainena (loc. 92)
Weighed
S LOWER
nt= 21
N
Ó1: 02/119
Ó2: 61/211
Ó3: 29/029
R, Ó': .36 8.52
Pure STRIKE-SLIP
Ó (°)
60
30
0
0 frequency x weight 16
V
Garrucha
2
P
S
1
G

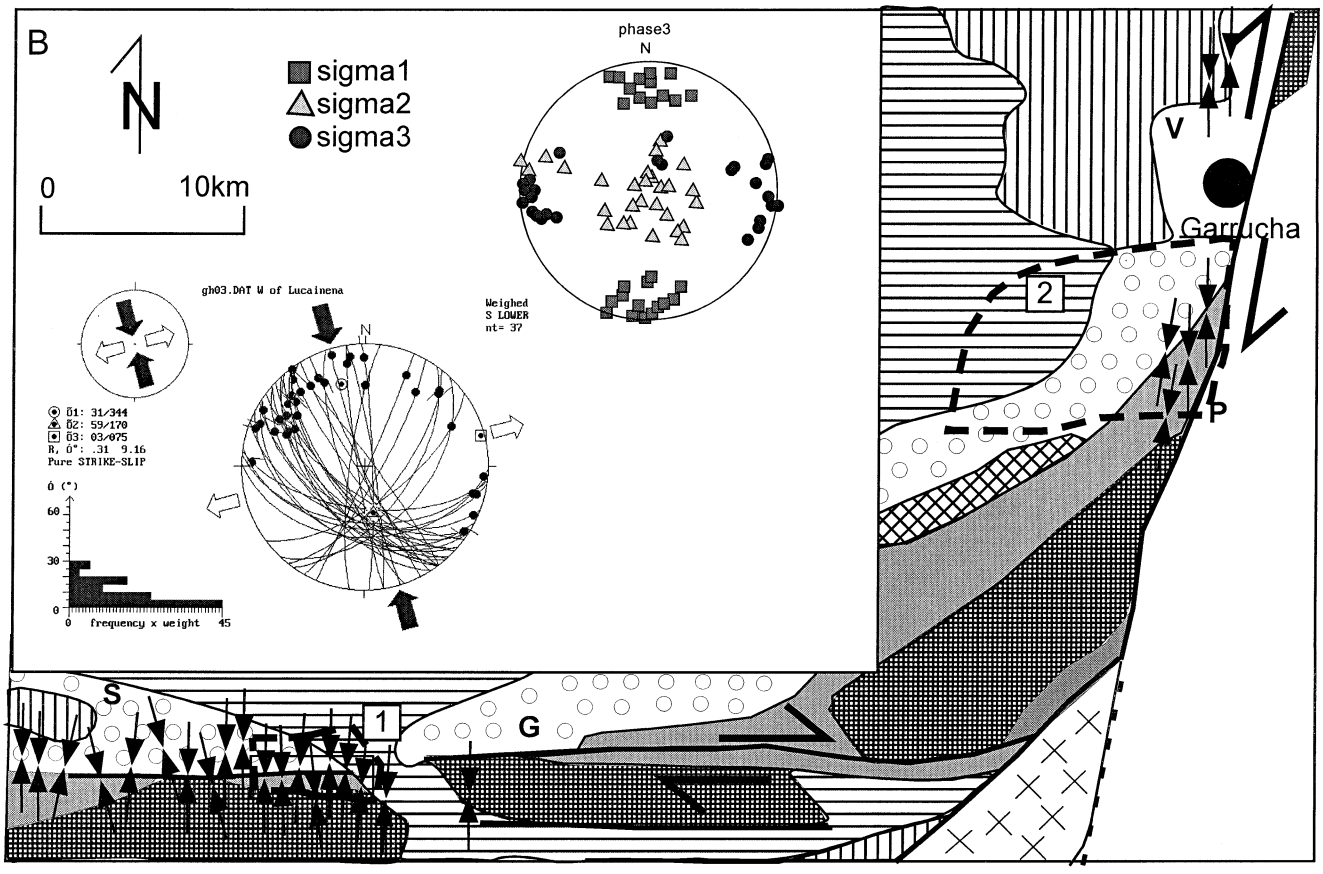
B
sigma1
sigma2
sigma3
0
10km
phase3
N
gh03.DAT W of Lucainena
Weighed
S LOWER
nt= 37
N
Ó1: 31/344
Ó2: 59/170
Ó3: 03/075
R, Ó': .31 9.16
Pure STRIKE-SLIP
Ó (°)
60
30
0
0 frequency x weight 45
V
Garrucha
2
P
S
1
G

Table 2
All tensors of phase 3. Symbols explained in text

Lithology	Structural location	N	N_{tot}	σ_1	σ_2	σ_3	α	TQR	Rank
Tort. turbidites	Gafarillos fault	14	25	354/14	106/59	255/29	9.83	0.81	B
Alp. basement	Gafarillos fault	8	27	185/14	005/76	096/00	3.90	0.61	B
Alp. basement	Gafarillos fault	18	25	001/09	222/78	092/08	10.7	1.09	B
Tort. turbidites	Gafarillos fault	14	20	187/06	337/85	097/04	10.9	0.70	B
Tort. turbidites	Gafarillos fault	16	20	178/07	048/79	269/08	8.29	1.55	A
Tort. turbidites	Gafarillos fault	17	43	349/20	215/62	086/18	11.5	0.60	B
Tort. turbidites	Gafarillos fault	11	27	009/27	217/61	105/12	8.76	0.53	B
Serr. conglom.	Gafarillos fault	12	15	181/06	068/75	272/13	7.54	1.27	B
Tort. turbidites	Gafarillos fault	23	30	025/19	283/30	142/54	12.6	1.27	B
Tort. turbidites	Gafarillos fault	37	40	344/30	170/60	075/03	7.83	3.64	A
Tort. turbidites	Gafarillos fault	10	15	180/32	012/59	274/05	7.66	0.87	B
Tort. turbidites	Gafarillos fault	20	30	346/09	212/78	077/08	9.70	1.36	B
Tort. turbidites	Gafarillos fault	21	27	175/11	013/78	265/04	9.72	1.67	A
Serr. conglom.	Gafarillos fault	16	19	199/02	301/78	109/11	6.54	2.03	A
Tort. turbidites	Gafarillos fault	29	53	355/29	137/56	255/18	11.4	1.34	B
Tort. turbidites	Gafarillos fault	11	22	161/22	011/63	257/12	5.78	0.70	B
Alp. basement	Unknown fault	14	62	001/16	147/71	268/10	9.14	0.54	B
Volcanites	Palomares fault	21	27	002/33	142/50	258/20	9.98	1.63	A
Alp. basement	Palomares fault	17	30	172/13	283/57	075/30	5.80	1.47	B
Alp. basement	Palomares fault	21	42	017/29	230/58	116/16	9.12	1.15	B
Alp. basement	Palomares fault	17	32	341/06	242/60	075/30	6.71	1.35	B
Alp. basement	Palomares fault	9	33	179/34	276/10	019/53	4.60	0.55	B
Alp. basement	Palomares fault	16	26	198/12	088/60	294/27	5.96	1.65	A
Volcanites	Palomares fault	20	30	167/16	260/11	023/70	10.5	1.25	B
Azagador/Abad	Polopos fault	18	29	194/21	284/00	014/69	9.93	1.14	B
Messinian	Polopos fault	13	25	011/08	280/06	154/80	10.5	0.63	B

Alpujarride basement and in Neogene sediments from Tortonian to earliest Messinian (Azagador member) age and not in younger rock units. This clearly illustrates that this stress-field did not persist in late-Messinian to Recent times. These results are in agreement with those obtained by Stapel et al. (1996) and Huibregtse et al. (1998).

3.2.3. Stress-tensors with a N–S trending σ_1 (phase 3 tensors)

Tensors of phase 3 are dominant throughout the study area. This tectonic phase, detected in a total number of 26 tensors, is characterized by a subhorizontal N–S trending maximum principal axis of compressive stress σ_1 and a subhorizontal E–W trending minimum principal axis of stress σ_3 (Table 2; Fig. 4b). These tensors are present in pre-Neogene Alpujarride basement and in Neogene sediments of Tortonian to late Messinian age as well as in Neogene volcanics, cropping out in the Vera Basin along the Palomares fault zone. The presence of this tensor confirms earlier results obtained by Stapel et al. (1996) and Huibregtse et al. (1998), who stated that a sudden change in the state of stress from phase 2 to phase 3 occurred in earliest Messinian time.

3.2.4. Stress-tensors with a subvertical σ_1 (phase 4 tensors)

Eight stress-sites are characterized by tensors with a subvertical σ_1 (Fig. 5). These tensors have been collected in Nevado–Filabride and Alpujarride basement-units, as well as in Neogene sediments and volcanites. σ_2 and σ_3 axes are subhorizontal, but vary in trend, which makes evaluation of this tensor difficult. Nevertheless, field-observations of normal-faulting overprinting strike-slip faulting, as well as the documentation of this tensor in previous studies (Stapel et al., 1996; Huibregtse et al., 1998), suggests that a tensional stress field existed in post-Miocene times.

4. Structural analysis

4.1. Deformation near the fault zones

Much information on the displacement history along the major strike-slip fault zones can be found in the deformational patterns of basin sediments adjacent to these fault zones. A fault zone is the central discontinuous part of a brittle-ductile shear-zone (Ramsay, 1980). A brittle-ductile shear-zone is defined as the total region within

Fig. 4. (a) Locations of phase 2 tensors in the studied areas. Upper stereonet shows all tensors of phase 2, lower stereonet shows one example of a phase 2 tensor. Dashed boxes 1 and 2 indicate the location of Figs. 6 and 7, respectively. Notations are the same as for Fig. 1. (b) Locations of phase 3 tensors in the studied areas. Upper stereonet shows all tensors of phase 3, lower stereonet shows one example of a phase 3 tensor.

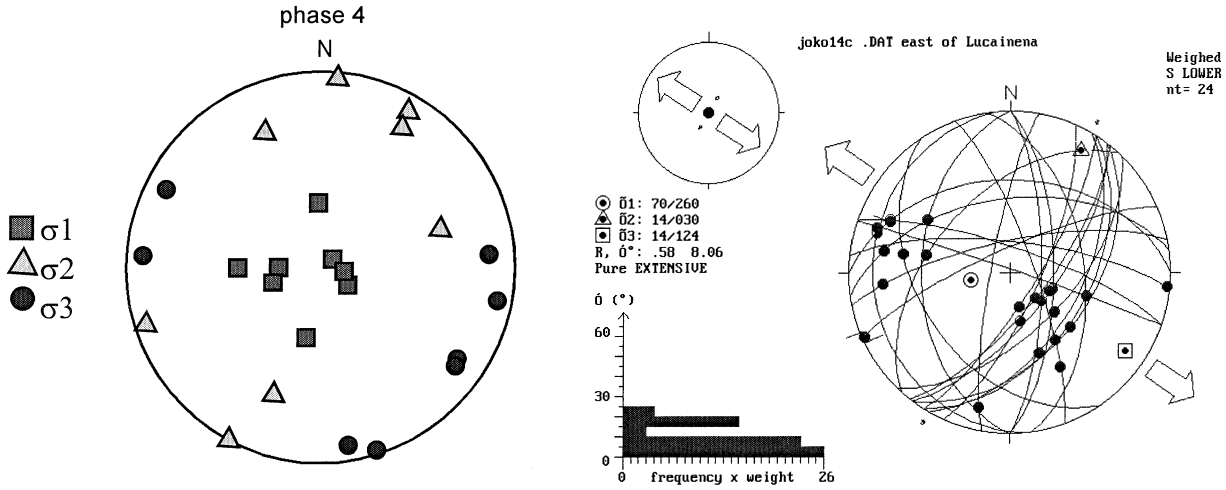

Fig. 5. Stress-tensors of phase 4 (left) with an example of a phase 4 stress tensor (right).

which deformation and rotation is coupled to the incremental strain-axes of a simple shear-zone. These incremental strain conditions, reflected in a simple-shear mechanism, have been treated theoretically by Ramsay (1980). For a two-dimensional case, without changes in volume, the shear strain γ is given by:

$$\gamma = \tan\psi \tag{3}$$

A circle, with unit-radius, is deformed to a strain-ellipse with principal axial half-lengths of $(1 + e_1)$ and $(1 + e_3)$. The axial half-lengths are conventionally expressed as quadratic elongations, λ_1 and λ_2 being $(1 + e_1)^2$ and $(1 + e_3)^2$, respectively. The strain-values for the long and short axes of the strain-ellipse are given by:

$$\lambda_1 = \tfrac{1}{2}(2 + \gamma^2 + \gamma(\gamma^2 + 4)^{\frac{1}{2}}) \tag{4}$$

$$\lambda_2 = \tfrac{1}{2}(2 + \gamma^2 - \gamma(\gamma^2 + 4)^{\frac{1}{2}}) \tag{5}$$

The orientation θ' of the principal strains measured from the x-coordinate direction is given by:

$$\tan 2\theta' = 2/\gamma \tag{6}$$

setting the positions of the principal strain axes for the incremental strain-ellipse at 45° and 135° to the x-coordinate axis. Structures such as folds and tension gashes will develop according to these orientations. Passive markers within the rock-body are rotated due to simple-shear. The relation between the original angle α between the marker and the shear-direction and the rotated angle α' is given by:

$$\cot\alpha' = \cot\alpha + \gamma \tag{7}$$

This last formula enables us to calculate shear-strain values for rotated markers in the field. In order to do this, we must know the present orientation as well as the original orientation of the rotated marker.

4.2. Deformation in the Sorbas Basin, adjacent to the Gafarillos fault zone

The sediments of the Sorbas Basin north of the central Gafarillos fault zone show deformation consistent with finite strain produced in a right-lateral shear-zone, with increasing (shear) strain and clockwise rotation of structures towards the central, brittle fault zone (Fig. 6). The main structures within the basin-sediments are folds, *Y*-shears, *R* and *R′*-shears, all of which can be linked to a right-lateral simple-shear model (Tchalenko, 1970). Fig. 6 shows NE–SW trending folds at distances of more than 500 m from the fault zone, while towards the fault zone, fold orientation gradually changes to E–W. These folds are dominant in sediments of Serravallian to Early Tortonian age. Sediments of younger Tortonian age, unconformably lying on top of older sediments show this pattern to a much lesser degree. Sediments of Messinian and younger age, known throughout the entire basin, show open E–W trending folds. Stapel et al. (1996) suggest that folding patterns throughout the entire Sorbas Basin are more or less E–W trending and can be related to phase 3 tensors. This may be true for sediments of younger Tortonian (and younger) age. The E–W trend of folds near the main fault zone in older sediments, however, is of a different origin. First of all, NE–SW trending folds gradually rotate clockwise towards E–W trending folds near the fault zone, with an associated decrease in wavelength and increase in tightness. Furthermore, NE–SW trending folds have not been observed at distances of over 1 km away from the main fault zone. This clearly suggests that these folds are related to the main fault zone, rather than being formed as regional folds. These folds were initiated parallel to the incremental maximum stretching direction within a right lateral shear-zone and we can calculate the amounts of shear strain from the rotation of these fold-hinges (Eq. (7)) and calculate a shear strain-distance profile across the shearzone (Ramsay and Graham, 1970; Weijermars, 1987). The orientation of

the fold-axes more than 500 m away from the Gafarillos fault zone is 048/02 (Fig. 6). This value corresponds to a high degree with the theoretical fold-axes of 045/00 for the incremental strain ellipse of the simple-shear model. Towards the main fault zone, fold-hinges progressively rotate clockwise to become 088/03 at distances of less than 100 m from the fault zone. From Eq. (7), our shear strain increases from 0 to 28 close to the fault zone. The same rotational patterns are difficult to see south of the main fault zone, within the basement-units. The transposition-foliation of the basement complexes shows two distinctly differently oriented fold axes. Plunge and trends of S_x-fold hinges for the Alpujarride and Malaguide units, situated directly against the fault zone, are 088/01, trends for the more southerly lying Nevado–Filabride complex are 001/02 (Fig. 6). On a few locations along the contact between the two units, a rigorous clockwise rotation of 87° of the Nevado–Filabride S_x N–S orientation is observed. This, together with the characteristic anastomosing patterns of an E–W trending shear-zone within the Alpujarride–Malaguide unit, suggests that the E–W orientation of the foliation of this complex is caused by the same simple-shear model as proposed for the basin sediments. E–W trending boudins of more competent dolomite and quartzite units more or less float in a matrix of phyllites. They are clearly stretched into the direction of the shearzone and compressed in the perpendicular direction, as would be expected for a simple-shear mechanism with high amounts of shear strain. The maximum shear strain for the basement complexes based on the rotation of the fold hinges is 57 (Eq. (7)).

If we assume that rotation of folds and basement reflects only simple-shear, we can construct a shear strain-distance profile across the Gafarillos shear-zone. This profile is asymmetric, with shear strain in basin sediments increasing from 0 to 28 at the fault-contact, rising to 57 within the basement rocks, before decreasing dramatically at the Alpujarride Nevado–Filabride contact (Fig. 6).

4.3. Deformation in the Vera Basin, adjacent to the Palomares fault zone

A similar analysis can be carried out for the Palomares shear-zone (Fig. 7). Sediments in the southeastern Vera Basin, north of the Sierra Cabrera and west of the main Palomares fault zone are of the Chozas and Turre Formation (Fig. 2). The structural map of this zone has been compiled from maps by Völk (1967) and our own mapping. This map presents one half of the total shear-zone; the eastern half is located in the Mediterranean Sea. The anti-clockwise rotation of basin fold-hinges into the main fault zone is clear. Another important aspect of the timing of movements is the angular unconformity between the Chozas and Turre Formation. Folds are only present within the Chozas Formation and are unconformably overlain by tilted (but not folded) sediments of the younger Turre Formation. The age of the folding is constrained by the stratigraphical gap between these two formations; folding must have taken place between 7 and 8 Ma. Despite this accurate timing, additional information on the kinematics of these folds cannot be found. We don't know whether these folds are related to the Palomares shear-zone or are regional folds. Nevertheless, shear strain values can still be calculated for the anti-clockwise rotation of these folds and bedding traces, as was previously done by Weijermars (1987). The angle between the shear-direction (the orientation of the Palomares fault zone) and the fold-axes at distances of more than 3 km away from the central fault zone is about 55°. The same angle reduces as a consequence of anti-clockwise rotations to about 10° close to the central fault zone (Fig. 7). A maximum shear strain of 5.0 is obtained from Eq. (6). A shear strain profile for the western half of the Palomares fault zone is shown in Fig. 7. The values obtained are slightly higher than those calculated by Weijermars (1987).

5. Discussion

5.1. Effect of rigid body rotation on shear strain calculations

The values for shear strain calculated from rotated fold hinges of both pre-Neogene basement units and Neogene sediments along both fault zones seem abnormally high, despite the orientation of the fold hinges being readily explained by a simple-shear mechanism. While the concepts may be reasonable for true 'ductile' shear-zones (Ramsay and Graham, 1970), the same mathematical methods may not apply to brittle-ductile shear-zones (Weijermars, 1987).

We argue that rigid body rotations are the prime cause of hinge line deflections. A better way to deal with the concept of shear-strain is provided here, in which the effect of rigid body rotations as the main component of the total sum of rotations is shown to be very important (Fig. 8). The total sum of rotations is given by rigid-body and non-rigid-body rotations. In our analysis, rotations caused by simple shear, in which shear strain values increase towards the main fault zone (in the centre of the shear-zone), are non-rigid-body rotations. The implication of high shear strain values is best illustrated by the shape of the 2D finite strain ellipse, which shows shortening to 1/30th of the original lengths for shear strain values of about 30. Such shortening was not observed in the field. To demonstrate that rotations near fault zones are largely rigid body and that amounts of (shear) strain are being over-estimated, we compare the values of the maximum shortening axis of the (shear) strain ellipse, as theoretically determined from shear strain values in the previous paragraphs, with observed shortening from field-data. We treat folds rotating as material lines (Jamison, 1991) rather than tracking the finite strain ellipse (Treagus and Treagus, 1992) which gives rise to small deviations between fold-axis orientation and the orientation of the

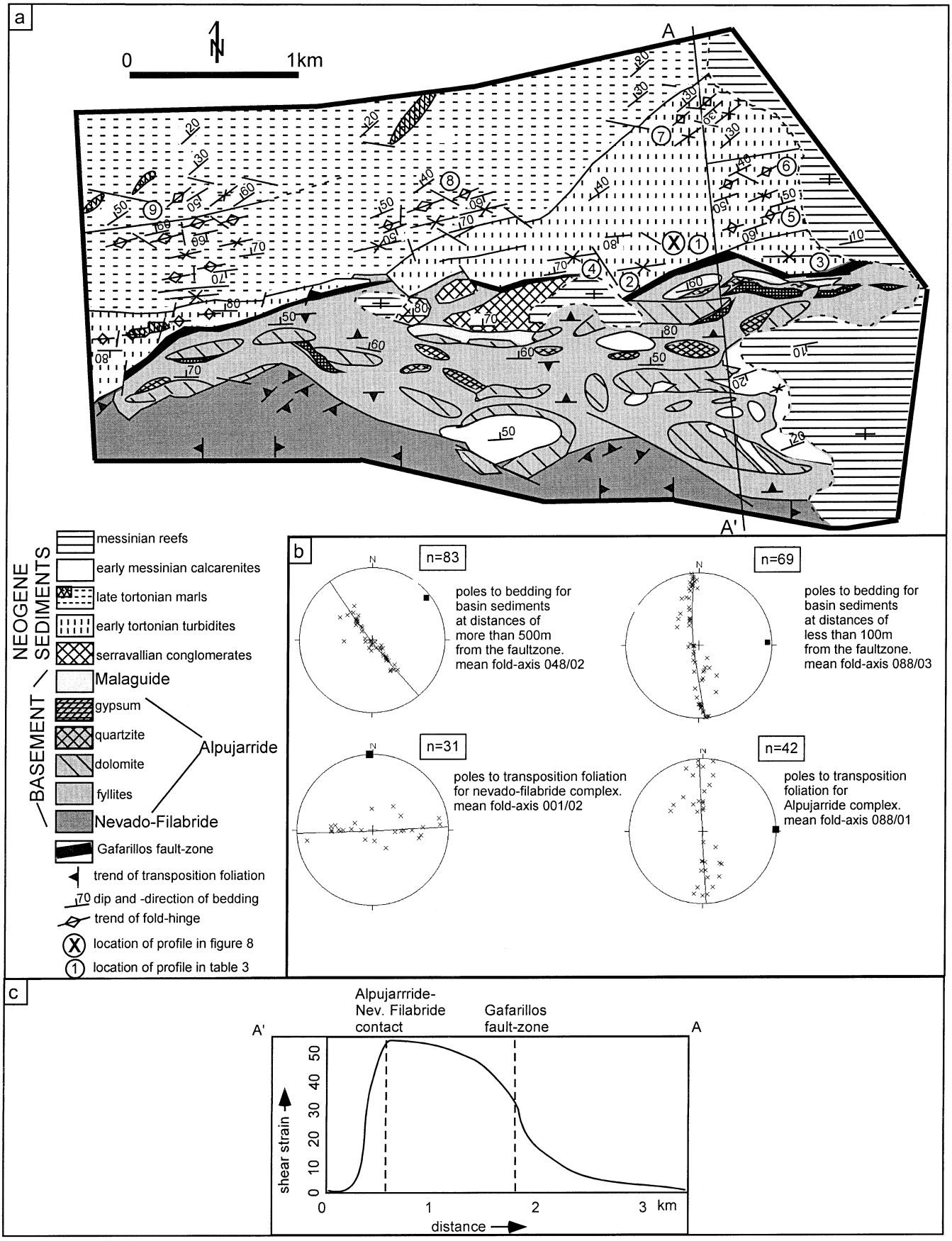
a
0
1km
A
A'
NEOGENE SEDIMENTS
messinian reefs
early messinian calcarenites
late tortonian marls
early tortonian turbidites
serravallian conglomerates
BASEMENT
Malaguide
gypsum
quartzite
dolomite
fyllites
Alpujarride
Nevado-Filabride
Gafarillos fault-zone
trend of transposition foliation
dip and -direction of bedding
trend of fold-hinge
location of profile in figure 8
location of profile in table 3
b
n=83
poles to bedding for basin sediments at distances of more than 500m from the faultzone. mean fold-axis 048/02
n=69
poles to bedding for basin sediments at distances of less than 100m from the faultzone. mean fold-axis 088/03
n=31
poles to transposition foliation for nevado-filabride complex. mean fold-axis 001/02
n=42
poles to transposition foliation for Alpujarride complex. mean fold-axis 088/01
c
A'
Alpujarrride-Nev. Filabride contact
Gafarillos fault-zone
A
shear strain
0 10 20 30 40 50
0 1 2 3 km
distance

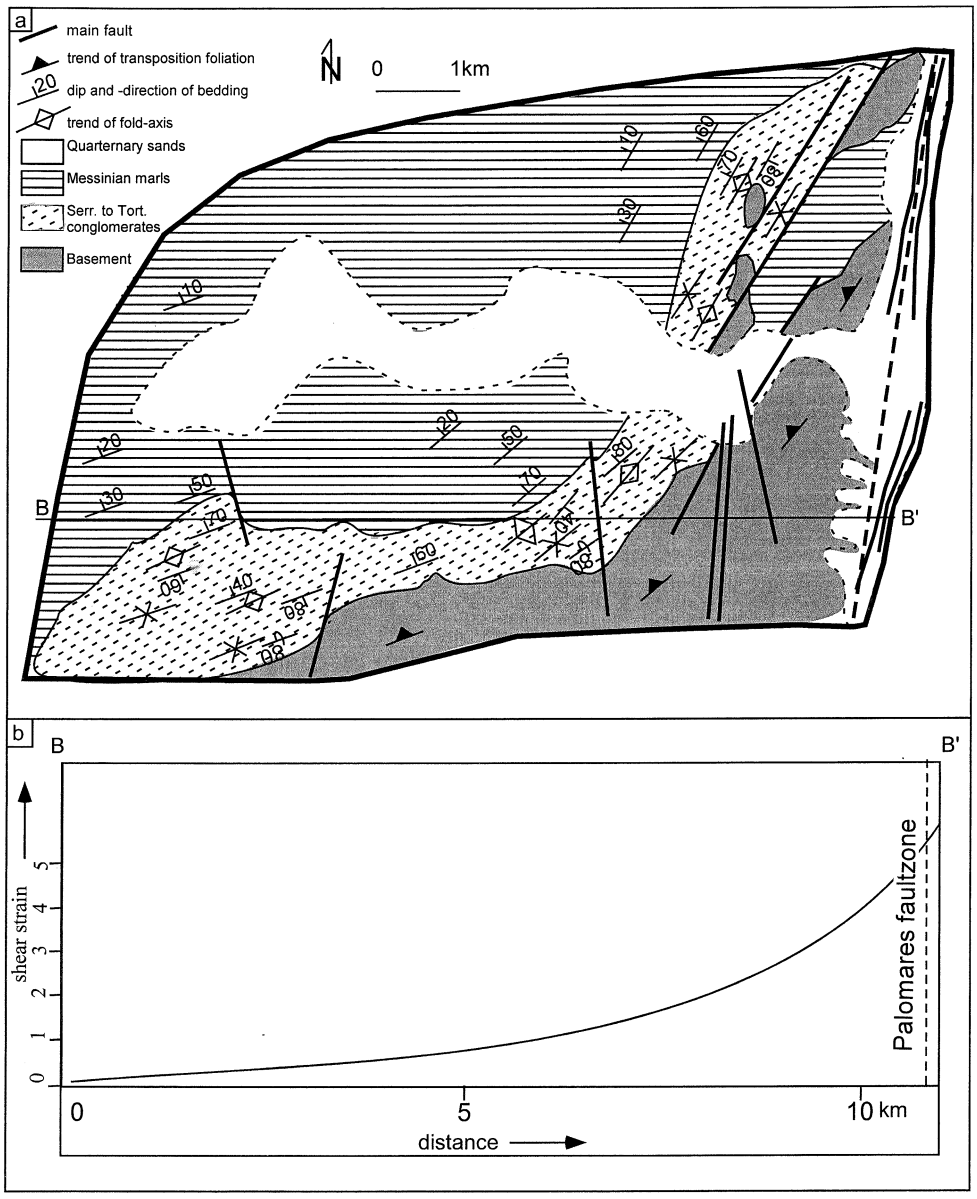

Fig. 7. (a) Structural map of area in box 2 of Fig. 4 (modified after Völk, 1967) showing main structural elements. (b) Shear strain-distance profile along line B–B′ (Fig. 7a) calculated from the rotation of fold-hinges.

axis of finite maximum shortening (Fig. 8b). The difference in shortening of folds treated as material lines and the theoretical maximum finite shortening are negligible for the understanding of the problem treated here. A detailed analysis of the question how fault-related folds are initiated and rotate (e.g. Tikoff and Peterson, 1998) is beyond the scope of this study.

For the Gafarillos shear-zone, the total amount of shortening is accommodated by folding. Shortening in small profiles (less than 10 m in length) perpendicular to fold-hinges, in which the fold-hinge orientation is more or less constant, can be calculated. Small profiles oriented normal to mean fold-axes should be shortened by a finite amount corresponding to a shear strain of 26. Let's consider a small profile *X* along the Gafarillos shear-zone (Figs. 6 and 8). The calculated value of shear strain from the rotation of fold axes of this location is 26. The shortening *e* from the profile is: $(l_f - l_0)l_0 = (7.5 - 20.5)/20.5 = -0.63$, with l_f

Fig. 6. (a) Structural map of area in box 1 of Fig. 4 showing main structural elements. (b) Equal area stereographic projections of poles to bedding of basin sediments and poles to transposition foliation of basement rocks in different parts of the studied area. Mean fold axes of the different domains are indicated with black squares. (c) Shear strain-distance profile (A–A′ in Fig. 6a) calculated from the rotation of fold-hinges.

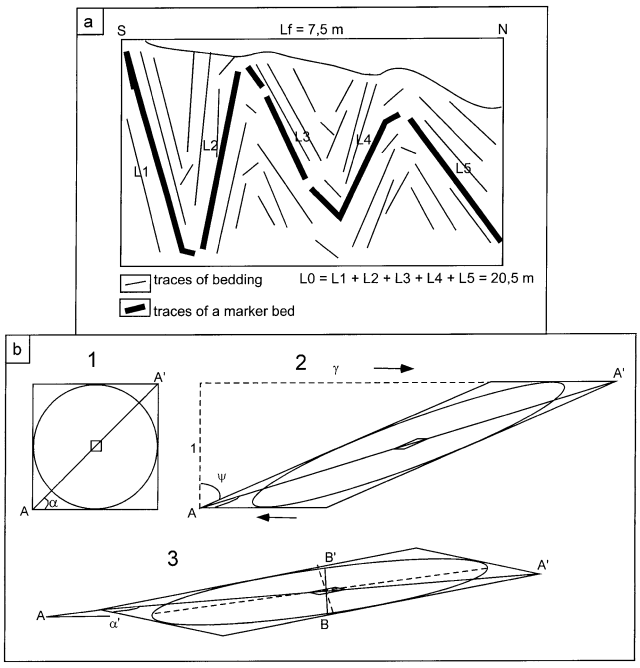

Fig. 8. (a) Profile *X* (location in Fig. 6) from which the shortening caused by folding was calculated. Original length $L_0 = 20.5$ m Final length $L_f = 7.5$ m. (b) Sequence of events for profile *X*: (i) The original undeformed situation, in which fold axes (material line A–A′) are developed at an angle of 45° with the shear direction. (ii) The result after a shear strain of 2.3 has been applied. (iii) The final orientation of fold axes, in which case a rigid body rotation of 10° has occurred. Fold-hinge A–A′ makes an angle of just 2° (α') with the shear direction. Shear strain was computed from the shortening of profile B–B′. Note that the orientation of the finite strain-axis of maximum shortening (dashed) is not completely perpendicular to the fold-hinge trend (solid), giving rise to small errors that for our purposes are not significant.

being the current length of the folded profile and l_0 being the original length of the unfolded profile (Fig. 8):

The quadratic elongation $\lambda_2 = (1 + e)^2 = 0.14$
The shear strain γ is then given by Eq. (5): $\gamma = 2.3$

The shear strain value, as calculated from the observed shortening, is roughly a factor of 10 smaller than the value calculated from the angular relationship. Calculations on several profiles (Table 3) show that these factor of 10 decreases occur on average throughout all profiles. From this observation, we must conclude that rigid-body-rotations played a major part in rotating markers within the shear zone with little accompanying internal deformation. Non-rigid-body rotations (the simple-shear model) can still be used to explain the deformational patterns, but play only a small part in rotating markers. The amount of rigid body rotations can be calculated using Eq. (6), in which case the amount of non-rigid-body rotations related to the shear strain of 2.3 diminishes to about 30°. The total rotation of about 40° is thus still largely a non-rigid-body rotation, but the added rigid body rotational effect greatly decreases the apparent calculated shear strain. The same holds for the 'Palomares shear-zone'. A comparison of the amount of shortening for different rotational domains, shows that the strongly rotated parts are not substantially shortened by larger amounts (Fig. 7). Again, most or perhaps all of the anti-clockwise rotations are rigid-body rotations.

5.2. Deformation and rotation in strike-slip shear-zones; a model of the Gafarillos shear-zone

Fig. 9 shows a model for deformation within basin sediments along the northern side of the Gafarillos fault, which incorporates fold-hinge orientations and shortening produced by folding as deduced from field-data. The width of the shear-zone north of the central fault-trace is about 1 km. In the first stage, folds related to dextral simple shear initiate within the shear-zone adjacent to the central fault at angles of 45° to the shear zone. Due to simple-shear deformation, these folds rotate clockwise and accommodate increasing shortening with increasing shear strain. The amount of shear strain increases to values between 2.0 and 2.5 close to the central fault-trace, as determined from the observed shortening caused by folding (Fig. 9a). With ongoing deformation, sinistral strike-slip faults develop more or less perpendicular to the shear direction. These faults cause progressive clockwise rigid body rotation of domains. Together with faults parallel to the shear direction (*Y*-shears) they define domains. Obviously, in the model, space problems are created along *Y*-shears. E–W trending lineaments observed along the Gafarillos fault-zone that decouple different domains consist of zones up to several meters thick that are intensely faulted. Space problems seem to be accommodated in these zones of intense brittle deformation. While the domains cease to deform internally, boundaries paralleling the shear direction will be focused sites of intense brittle deformation, with the central fault-trace marking the zone of most intense cataclastic deformation. From field-data, it is observed that folding predates major faulting and fold-hinges show much larger amounts

Table 3
Shear strain values from fold-hinge rotations compared with those from shortening normal to fold-axes suggests that rigid-body-rotations play a major role in translations. Location numbers shown in Fig. 6

Location number	1	2	3	4	5	6	7	8	9
γ from rotations of fold-axes	26	28	29	27	25	20	14	11	7
γ from shortening normal to fold-axes	2.1	3.1	3.3	3.1	1.8	1.6	1.5	1.5	1.0

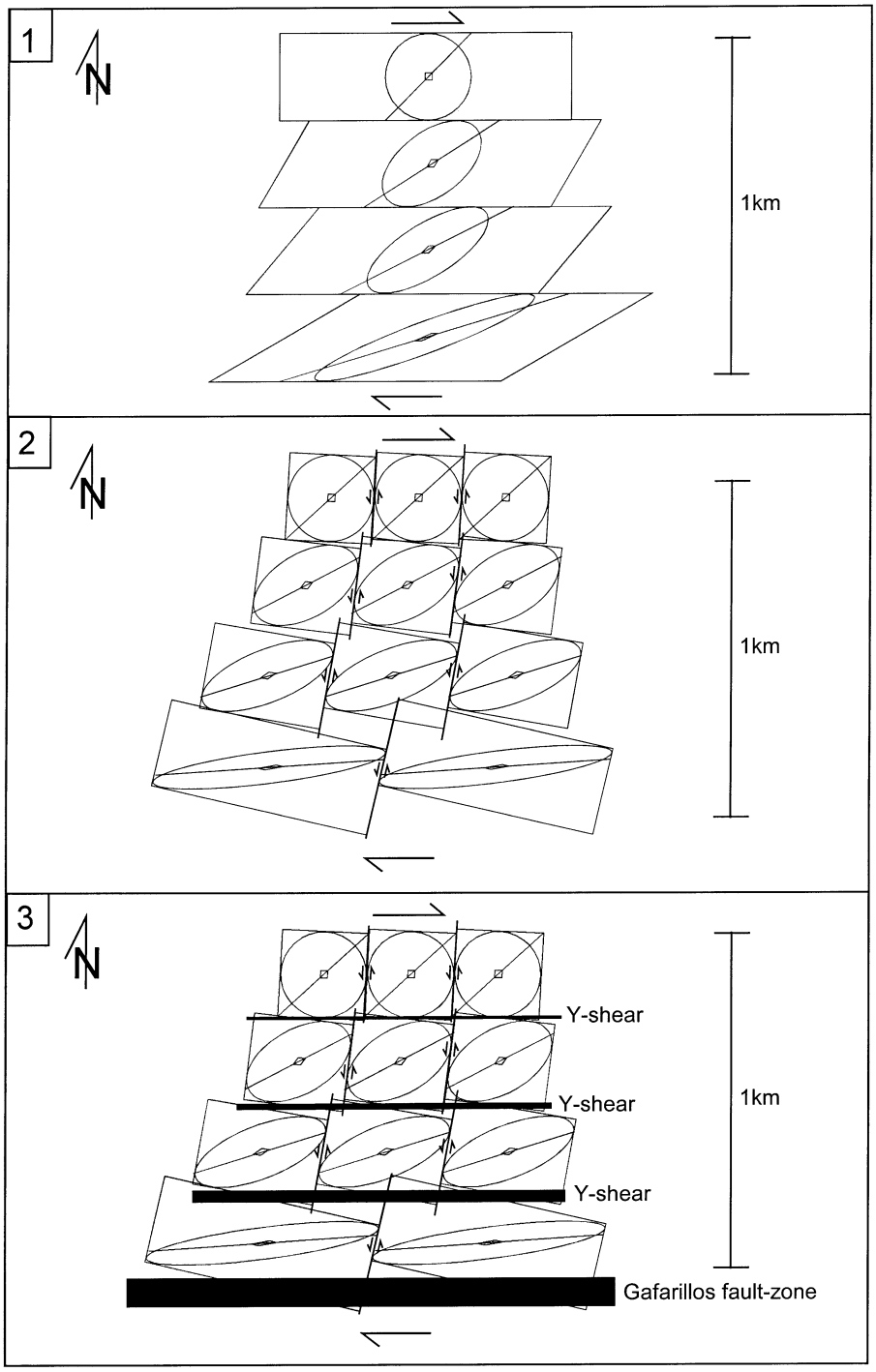

Fig. 9. Cartoon illustrating the styles of deformation and rotation within the northern half of the Gafarillos shear zone (Fig. 6). (a) Folds related to dextral simple shear develop at angles of 45° to the shear-zone and progressively rotate due to simple shear deformation with values up to about 2.3 close to the central fault-trace. (b) To accommodate further rotation, distinct domains develop, separated by sinistral strike-slip faults at high angles to the shear-zone direction. Distinct blocks rotate rigidly due to movements along these sinistral strike-slip faults. (c) To account for space problems created by increasing rigid body rotation close to the central fault-trace, zones parallel with the shear-zone direction develop. These zones do not accommodate large amounts of displacements, but do consist of localized strongly brittle-deformed rock caused by differential rigid body rotation of domains.

of rotation than faults, which is readily explained by the fact that faults post-date simple-shear deformation and non-rigid body rotation, accommodating only the smaller component of rigid body rotation.

5.3. Transpression-tectonics; an alternative model

Sanderson and Marchini (1984) use the transpression model to explain en échelon folds from southern California

(Moody and Hill, 1956) with orientations at low angles to associated faults in order to avoid incorporating high shear strain values. Obviously, this model may be applied in this case to explain fold-initiation at low angles to bounding faults and transpression tectonics have been previously reported along strike-slip faults in the Betics of SE Spain (Carboneras fault; Keller et al., 1995). Progressive rotation of folds near faults may be explained by simple shear deformation or by incorporating increasing components of pure shear (transpression) near the fault. However, the amounts of pure shear deformation needed to explain fold orientations almost parallel to faults would require much larger amounts of shortening caused by folding than observed from field-data. In our case, there is a clear clockwise rotation of folds initiated at 45° away from the central fault-trace towards orientations almost parallel to the central fault-trace adjacent to it (right-lateral Gafarillos fault-zone). Along the left-lateral Palomares fault-zone, a clear anti-clockwise rotation of folds is observed (Weijermars, 1987; this study). These progressive rotations, consistent with the sense of motion along the bounding faults, can only be explained by introducing large components of rigid body rotation. Furthermore, several paleo-stress studies along differently oriented fault-zones in the area (Stapel et al., 1996; Huibregtse et al., 1998; this study) have yielded a considerable data-base showing the presence of two main tensors related to strike-slip deformation in the Internal Zone (tensors of phases 2 and 3 in this study). Age relations have shown that these are two phases in time rather than in space. Thus, consistent paleo-stress orientations prevailed in space. If increasing components of transpression and transtension prevailed along fault-zones, this should be reflected in curving paleo-stress orientations closer to faults. We do not completely rule out the possibility of a component of transpression along some faults, but their contribution will be small compared with the influence of rigid body rotation. Future work will need to focus on computing deformation matrices not only for discrimination between pure and simple shear (Fossen and Tikoff, 1993), but also incorporating rigid body rotations.

6. Conclusions

Important E–W directed compression dominated Langhian to Serravallian time. This E–W directed compression has been recorded along the Ramonete fault zone. Along the Ramonete fault zone, relics of Langhian to Serravallian red continental conglomerates and yellow marine marls are present. These units are intensely folded and faulted and intermixed as slivers with pre-Neogene basement units (Bon et al., 1989). Timing of this tectonic phase is well constrained by relatively undeformed Tortonian sediments, sealing the Ramonete fault zone north of Mazarron. This tectonic phase could represent the collision of the Betic subplate with the Iberian mainland (Sanz de Galdeano, 1990). During Tortonian to earliest Messinian time, the Betic Cordilleras were dominated by a strike-slip regime with a NW–SE oriented maximum principal axis of stress, allowing a large component of dextral shear along the E–W trending Gafarilllos fault zone. Tectonic phase 2 is dominantly present in the Sorbas basin adjacent to the Gafarillos fault zone. Movements along the Gafarillos fault zone produced deformation consistent with dextral simple shear on the fault. Rotations, however, are best explained taking large rigid-body components into account. Main movements along the Gafarillos fault zone occurred in the early Tortonian, as is evidenced by coverage of less disturbed upper Tortonian marls on top of highly folded and tilted lower Tortonian turbidites. Activity along this fault zone ceased during later Messinian time, as is evidenced by sealing of the fault zone by late Messinian reef carbonates. First indications for fault activity along the Palomares fault zone is given by the presence of rhyolitic to dacitic volcanism in the Vera basin (Völk, 1967; Nobel, 1981; Bellon et al., 1983). These volcanic bodies occur in a strike similar to the Palomares fault zone and are intruded along one of the fault-splays. Tortonian whole-rock ages for these volcanites were determined at 8.3 Ma (Bellon et al., 1983). Sinistral displacements along this fault zone occurred under the influence of phase 2 tensors. With the abrupt rotation of the stress-field, the 020 trending Palomares fault zone could still accommodate a large shear component paralleling the fault zone, causing sinistral strike-slip. The termination of sinistral strike-slip can be precisely determined from the presence of undisturbed Pliocene sediments overlying this fault zone. Anti-clockwise rotations of folds determine the width of the Palomares shear-zone. Again these rotations cannot be explained as non-rigid body rotations related to increased shear strains near the central fault zone. Normal faulting in Pliocene sediments records the subrecent tectonic regime, which confirm previous results obtained by Stapel et al. (1996) and Huibregtse et al. (1998). Apart from the precise dating of fault-movements, this study has also shown that shear strain values are highly overestimated when considering rotational effects to be caused purely by a simple shear-strain mechanism (Weijermars, 1987). Comparing orientations of fold-hinges with shortening caused by folding will lead to a better understanding of the different components of deformation and rotation involved in brittle-ductile shear-zones.

Acknowledgements

Bruis Gianotten, Vincent Helfferich, Robin Koelewijn, Menno Bantje and Dr Anne Fortuin are kindly thanked for their collaboration during fieldwork in the area in 1998. Our work greatly benefited from structural and stratigraphical work done by H.R. Völk (1967). Reviewers A. Nicol, R. Norris and A. Mather helped improving the paper.

References

Angelier, J., 1989. From orientations to magnitudes in paleostress determinations using fault slip data. Journal of Structural Geology 11, 37–50.

Bakker, H.E., De Jong, K., Helmers, H., Biermann, C., 1989. The geodynamic evolution of the Internal Zone of the Betic Cordilleras (south-east Spain): a model based on structural analysis and geothermobarometry. Journal of metamorphic Geology 7, 359–381.

Bellon, H., Bordet, P., Montenat, C.H., 1983. Chronologie du magmatisme néogène des Cordillères bétiques (Espagne méridionale). Bulletin de la Société Geologique de France 25 (7), 205–217.

Biermann, C., 1995. The Betic Cordilleras — anatomy of a dualistic collision-type orogenic belt. Geologie en Mijnbouw 74, 167–182.

Bon, A., Biermann, C., Koenen, D.B., Simon, O.J., 1989. Middle Miocene strike-slip tectonics in the Aguilas–Mazarron region. Proceedings van de Koninklijke Nederlandse Akademie voor Wetenschap Serie B 92 (2), 143–157.

Bott, M.H.P., 1959. The mechanics of oblique slip faulting. Geological Magazine 96, 109–117.

Delvaux, D., 1994. Tensor interactive MS-DOS Quick Basic program developed for paleostress determinations on geological fractures and earthquake focal mechanisms. Royal Museum for Central Africa, Tervuren, Version, 29.

Delvaux, D., Moeys, R., Stapel, G., Petit, C., Levi, K., Miroshnichenko, A., Ruzhitch, V., Sankov, V., 1997. Paleostress reconstructions and geodynamics of the Baikal region, Central Asia, Part II. Cenozoic tectonic stress and fault kinematics. Tectonophysics 282, 1–38.

Egeler, C.G., Simon, O.J., 1969. Sur la tectonique de la zone Bétique (Cordillères Bétiques, Espagne). Proceedings van de Koninklijke Nederlandse Akademie voor Wetenschappen, Afdeling Natuurkunde, eerste reeks 25, 1–90.

Fortuin, A.R., Kelling, J.M.D., Roep, T.B., 1995. The enigmatic Messinian–Pliocene section of Cuevas del Almanzora (Vera basin, SE Spain) revisited — erosional features and strontium isotope ages. Sedimentary Geology 97, 177–201.

Fossen, H., Tikoff, B., 1993. The deformation matrix for simultaneous simple shearing, pure shearing and volume change, and its application to transpression–transtension tectonics. Journal of Structural Geology 15 (3–5), 413–422.

Garcia-Hernandez, M., Lopez-Garrido, A.C., Rivas, P., Sanz de Galdeano, C., Vera, J.A., 1980. Mesozoic paleographic evolution of the External Zones of the Betic Cordilleras. Geologie en Mijnbouw 59, 155–168.

Geel, T., 1995. Oligocene to early Miocene tectono-sedimentary history of the Alicante region (SE Spain): implications for Western Mediterranean evolution. Basin Research 7, 313–336.

Haughton, P.D.W., 1994. Deposits of deflected and ponded turbidity currents, Sorbas Basin, southeast Spain. Journal of Sedimentary Research (A) 64, 233–246.

Huibregtse, P.W., van Alebeek, J.M., Zaal, M.E.A., Biermann, C., 1998. Paleostress analysis of the northern Nijar and southern Vera basin — constraints for the Neogene displacement history of major strike-slip faults in the SE Betic Cordilleras, Spain. Tectonophysics 300, 79–101.

Jamison, W.R., 1991. Kinematics of compressional fold development in convergent wrench terranes. Tectonophysics 190, 209–232.

Keller, J.V.A., Hall, S.H., Dart, C.J., McClay, K.R., 1995. The geometry and evolution of a transpressional strike-slip system: the Carboneras fault, SE Spain. Journal of the Geological Society of London 152, 339–351.

Kleverlaan, K., 1989. Tabernas fan complex — a study of a Tortonian Fan Complex in a Neogene basin, Tabernas, Province of Almeria, SE Spain. PhD Thesis, Vrije Universiteit, Amsterdam.

Mather, A.E., Harvey, A.M., 1995. Controls on drainage evolution in the Sorbas basin, southeast Spain. In: Lewin, J., Macklin, M.G., Woodward, J. (Eds.). Mediterranean Quaternary River Environments. Balkema, Rotterdam, pp. 65–76.

Moody, J.D., Hill, M.J., 1956. Wrench-fault tectonics. Bulletin of the Geological Society of America 57, 1207–1246.

Nobel, F., 1981. The age of veritic volcanites in SE Spain. MSc thesis, Universiteit van Amsterdam.

Postma, G., Roep, T.B., 1985. Resedimented conglomerates in the bottomsets of Gilbert-type gravel deltas. Journal of Sedimentary Petrology 55, 874–885.

Ramsay, J.G., 1980. Shear zone geometry: a review. Journal of Structural Geology 2, 83–99.

Ramsay, J.G., Graham, R.H., 1970. Strain variations in shear-belts. Canadian Journal of Earth Sciences 7, 786–813.

Ramsay, J.G., Huber, M.I., 1987. The Techniques of Modern Structural Geology, Volume 2: Folds and Fractures. Academic Press, London.

Sanderson, D.J., Marchini, R.D., 1984. Transpression. Journal of Structural Geology 6, 449–458.

Sanz de Galdeano, C., 1990. Geological evolution of the Betic Cordilleras in the Western Mediterranean, Miocene to the Present. Tectonophysics 172, 107–119.

Sanz de Galdeano, C., Vera, J.A., 1992. Stratigraphic record and paleogeographic context of the Neogene basins in the Betic Cordillera, Spain. Basin Research 4, 21–36.

Stapel, G., Moeys, R.P., Biermann, C., 1996. Neogene evolution of the Sorbas basin (SE Spain) determined by paleostress analysis. Tectonophysics 255, 291–305.

Sylvester, A.G., 1988. Strike-slip faults. Geological Society of America Bulletin 100, 1666–1703.

Tchalenko, J.S., 1970. Similarities between shear zones of different magnitudes. Geological Society of America Bulletin 81, 1625–1640.

Tikoff, B., Peterson, K., 1998. Physical experiments of transpressional folding. Journal of Structural Geology 20, 661–672.

Treagus, J.E., Treagus, S.H., 1992. Transected folds and transpression: how are they related?. Journal of Structural Geology 14, 361–367.

Völk, H.R., 1967. Zur Geologie und Stratigraphie des Neogenenbekkens vor Vera. Südostspanien. PhD. Thesis, Universtiteit van Amsterdam.

Völk, H.R., Rondeel, H.E., 1964. Zur Gliederung des Jungtertiars im Becken von Vera, Südost–Spanien. Geologie en Mijnbouw 64, 310–315.

Weijermars, R., 1987. The Palomares brittle-ductile Shear Zone of southern Spain. Journal of Structural Geology 9, 139–157.

Weijermars, R., Roep, T.B., Van den Eeckhout, B., Postma, G., Kleverlaan, K., 1985. Uplift history of a Betic fold nappe inferred from Neogene–Quarternary sedimentation and tectonics (in the Sierra Alhamilla and Almeria, Sorbas and Tabernas basins of the Betic Cordilleras, SE Spain). Geologie en Mijnbouw 64, 397–411.